RSC Advances

PAPER

View Article Online
View Journal | View Issue

Cite this: *RSC Adv.*, 2020, **10**, 27439

Cu/TCH-pr@SBA-15 nano-composite: a new organometallic catalyst for facile three-component synthesis of 4-arylidene-isoxazolidinones†

Mehdi Kalhor,* Seyed Mehdi Sajjadi and Akbar Dadras

A copper complex supported on SBA-15 nanoparticles (Cu/TCH-pr@SBA-15) was synthesized by the post-synthesis modification of nano-mesoporous silica with 3-chloropropyltriethoxysilane (CPTES) and thiocarbohydrazide (TCH) and subsequent metal–ligand coordination with Cu(II). These nanocomposites were thoroughly characterized by FT-IR spectroscopy, TEM, FE-SEM, EDX, atomic absorption spectroscopy and N_2 adsorption–desorption (BET) studies. Then, a solvent-free method was developed for the three-component synthesis of 4-arylidene-isoxazolidinones *via* condensation of hydroxylamine hydrochloride, ethyl acetoacetate and various aromatic aldehydes using Cu/TCH-pr@SBA-15 as a highly efficient nanocatalyst. This new economic and eco-friendly methodology has remarkable advantages such as excellent yields, a shorter reaction time, an easy purification procedure, simplicity, green conditions, solvent-free conditions, and recoverability of the nanocatalyst.

Received 11th February 2020
Accepted 28th June 2020

DOI: 10.1039/d0ra01314e

rsc.li/rsc-advances

1. Introduction

Isoxazole and its derivatives are very useful heterocycles, and are used to create synthetic pharmaceutical compounds.[1,2] They are widely recognized in the fields of medicine and organic chemistry due to their anti-inflammatory,[3] fungicidal,[4] antioxidant,[5] analgesic,[6] nematicidal,[7] antimicrobial,[8] antiviral,[2] and hypoglycemic activity.[9] Isoxazole-based drugs are used in both human and veterinary medicine (Fig. 1).[1,2] In this sense, synthetic methods aiming to achieve this heterocycle core is a permanent interest, and various protocols have been developed to accomplish this purpose.[5]

Isoxazole heterocycles are prepared through the one-pot reaction of an aldehyde, hydroxylamine hydrochloride and a β-ketoester using various catalytic systems.[10–18] In general, these methods have some disadvantages such as harsh reaction conditions, poor yields, difficult work-up procedures, long reaction times, and the use of organic solvents and expensive catalysts. Therefore, advanced synthetic procedures and catalytic methods are still needed for the efficient synthesis of isoxazole scaffolds.

Nowadays, there has been an ongoing effort to use homogeneous catalysts on supports in catalytic reactions. Supported catalysts have the advantages of both homogeneous catalysis and heterogeneous recycling. Among the appropriate supports, mesoporous silicate SBA-15 has attracted considerable attention because of its desirable characteristics such as regular channel nanostructures, large surface area, pore diameters in the range of 2 to 30 nm and tunable surface chemistry. Moreover, SBA-15 can be modified by organic and inorganic materials. Designing and modifying the surface of SBA-15 with organic and inorganic materials have attracted particular attention due to its high quantity of surface hydroxyl groups, which is a key factor for its application in catalytic processes. One of the convenient approaches for the functionalization of nano-porous SBA-15 involves anchoring the desired functionalities onto the mesoporous silica. In this case, a covalent interaction could be established between the organic functional group and the silica framework, which prevents leaching of the active centers from the catalyst surface in the reaction mixture. Therefore, heterogeneous catalysts bearing active metal centers supported on modified SBA-15 nanoparticles can be an ideal choice in catalytic systems.[19]

Copper atom species as homogeneous catalysts have been immobilized on a variety of supports, and their catalytic activities have been investigated for various organic reactions.[20–22] Well-dispersed Cu catalysts on suitable supports can enhance their catalytic activity. The advantages of SBA-15 make it an ideal support for the immobilization of Cu in order to develop an optimized heterogeneous catalyst. There are two methods for dispersing Cu on the surface SBA-15: the direct synthesis procedure[23] and post synthesis method.[24] Despite the availability of these methods, it remains a challenge to achieve a strong interaction between metal ions and ordered mesoporous SBA-15.[21] Therefore, the development of a new and efficient approach for stable grafting of Cu ions onto the SBA-15 surface is still required for catalytic organic transformation.

Department of Organic Chemistry, Payame Noor University, Tehran, 19395-4697, Iran. E-mail: mekalhor@gmail.com; mekalhor@pnu.ac.ir; Fax: +98 2537179170; Tel: +98 2537179170

† Electronic supplementary information (ESI) available. See DOI: 10.1039/d0ra01314e

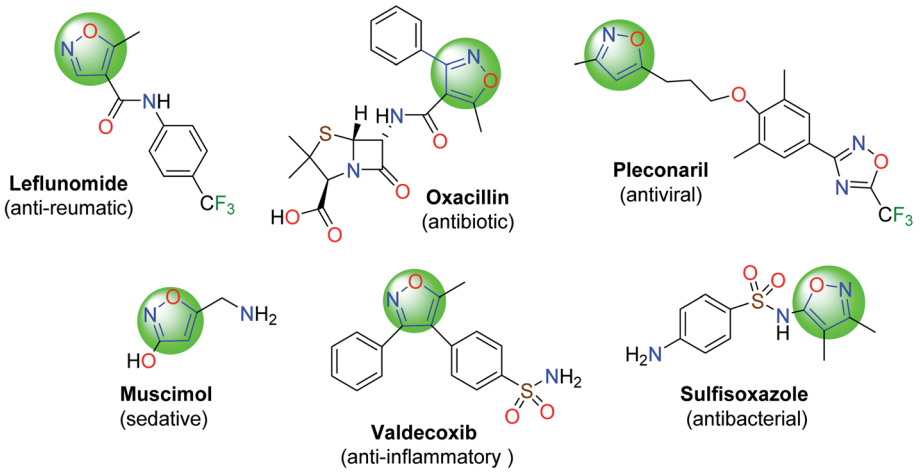

Fig. 1 Examples of the isoxazole-based drugs.

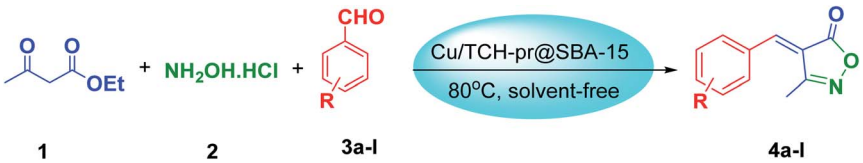

Scheme 1 The synthetic pathway of isoxazole-5(4*H*)-one derivatives.

For the above reasons, and in continuation of our research on the synthesis of new supported nanocatalysts,[25,26] we report herein a novel approach for the preparation of a stable and active Cu catalyst supported on functionalized SBA-15 nanoparticles for the synthesis of 3-methyl-4-arylmethylene isoxazole-5(4*H*)-ones *via* condensation of aldehyde derivatives with hydroxylamine hydrochloride and ethyl acetoacetate under solvent-free conditions (Scheme 1).

2. Experimental

2.1. Materials and apparatus

Chemical materials were purchased from Sigma-Aldrich and Merck and used as received without further purification. Melting points were determined in open capillaries using an electro-thermal digital melting point apparatus and are uncorrected. FT-IR spectra were recorded on a JASCO 4200-A spectrometer with KBr pellets. ^{1}HNMR and ^{13}CNMR spectra were recorded on a Bruker spectrometer (300–500 MHz) using DMSO-d_6 as the solvent and Me_4Si as the internal standard. The morphology of the functionalized SBA-15 was investigated using a Leica Cambridge S 360 scanning electron microscope (SEM and FTSEM). Transmission electron microscopy (TEM) images were recorded on a Philips CM10 with an acceleration voltage of 100 kV. N_2 adsorption–desorption isotherms of SBA-15 nanocomposites were measured at the temperature of liquid nitrogen with a Micromeritics system (made in USA). The BET surface area of the nanoparticles was calculated using the Brunauer–Emmett–Teller (BET) method.

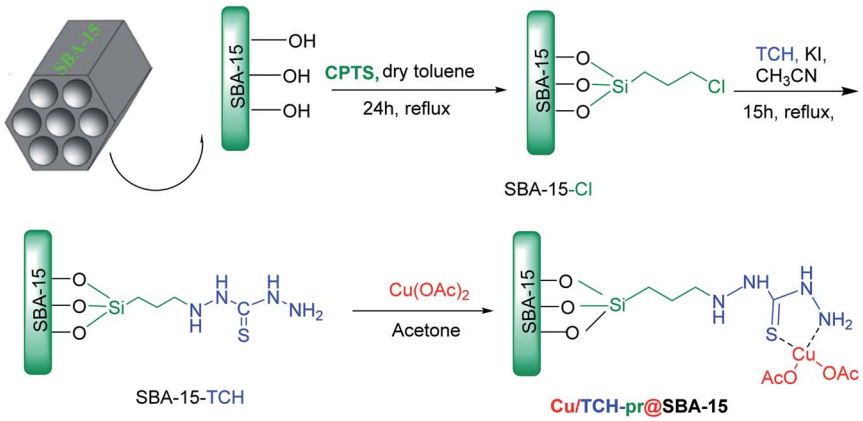

Scheme 2 Schematic diagram for the synthesis of Cu/TCH-pr@SBA-15 nanocatalyst.

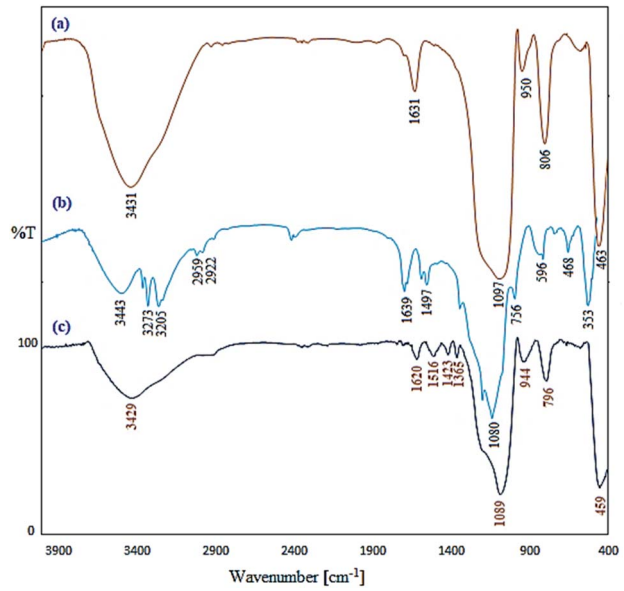

Fig. 2 FT-IR spectra of (a) SBA-15, (b) SBA-15-TCH, and (c) Cu/TCH@SBA-15.

2.2. Typical procedure for the synthesis of Cu/TCH-pr@SBA-15 nanocatalyst

The chloropropyl-functionalized nanoporous SBA-15 (SBA-15-Cl) was synthesized according to a literature procedure.[26] Then, for the synthesis of SBA-15-Cl modified with TCH (SBA-15-TCH), in a 100 ml round-bottom flask, 1.44 g (13.56 mmol) of TCH was dissolved in 21 ml of acetonitrile and stirred for 1 h. Next, 1.40 g (8 mmol) of KI and 1.43 g of SBA-15-Cl were added to the reaction mixture and refluxed for 15 h. Then, the solvent was removed and the mixture was collected by centrifuge. The obtained solid was stirred in 50 ml distilled water to remove the precursor residue, separated by vacuum filtration with a Buchner funnel, and dried in an oven at 50 °C for 12 h. For the immobilization of Cu(II) ions on the functionalized SBA-15, 0.17 g (0.9 mmol) of copper acetate was dissolved in 10 ml acetone, and 1.60 g of SBA-15-TCH was added to the solution and stirred at room temperature for 3 h. The mixture was filtered, washed with acetone and THF and dried in an oven at 40 °C for 3 h to produce Cu/TCH-pr@SBA-15.

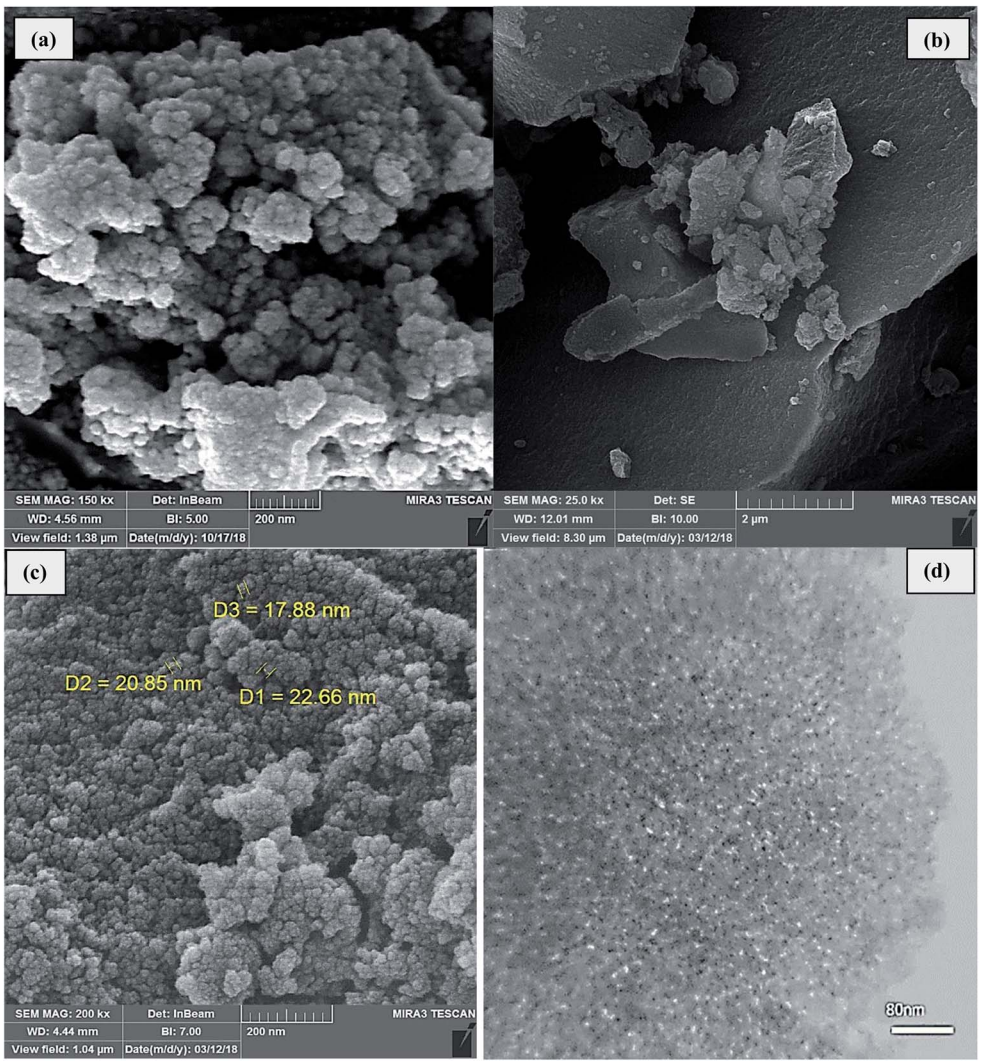

Fig. 3 FE-SEM images of (a) SBA-15-TCH, (b) and (c) Cu/TCH-pr@SBA-15 and TEM (d) image of Cu/TCH-pr@SBA-15.

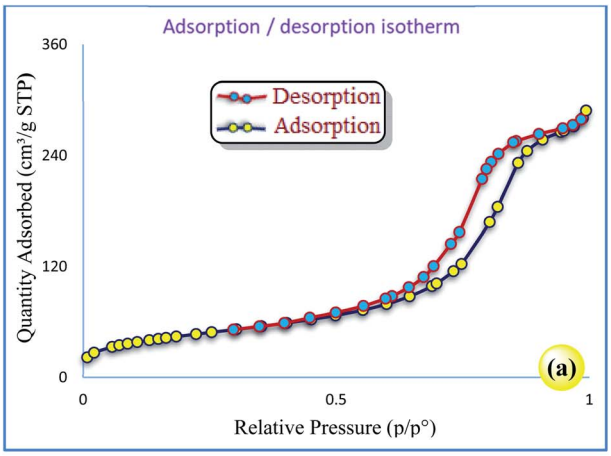

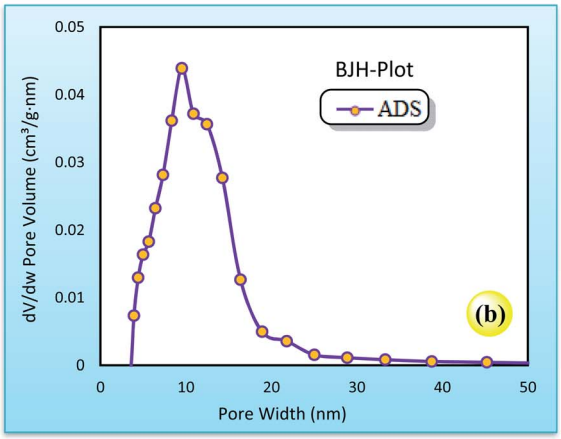

Fig. 4 (a) Adsorption/desorption N_2 isotherms and (b) pore size distribution of Cu/TCH-pr@SBA-15.

2.3. Solvent-free procedure for the preparation of 3,4-disubstituted isoxazole-5(4*H*)-one

A mixture of ethyl acetoacetate (1 mmol), Cu/TCH-Pr@SBA-15 (0.0032 g, 2.5% W) as catalyst, hydroxylamine hydrochloride (1 mmol) and aromatic aldehyde (1 mmol) was prepared and was stirred magnetically at 80 °C for 7–12 minutes (Table 3). The complete consumption of the starting materials was observed by TLC (*n*-hexane/ethyl acetate: 2 : 1 v/v). After completion of the process, the reaction mixture was dissolved in hot EtOH, and Cu/TCH-pr@SBA-15 was filtered off. 10 ml of cold water was added to the filtrate, and the resulting precipitate was obtained by filtration and washed with a cold ethanol–water mixture. The pure product was dried and identified by spectroscopic data and by comparing their melting points with literature values. The characterization data for some of the 3,4-disubstituted isoxazole-5(4*H*)-ones are given below.

Spectroscopic data for selected compounds

3-Methyl-4-benzylideneisoxazol-5(4H)-one (***4a***). FT-IR (KBr, ν_{max}): 3434, 3052, 2926 (CH), 1749, 1732 (C=O), 1655 (C=N), 1556, 1441 (C=C), 1217 (C–O), 1014, 812, 754, 571 cm^{-1}; ^1H NMR (300 MHz, DMSO-d_6): δ_H 8.41–7.21 (m, 6H, H–Ar and C=CH), 2.30 (s, 3H, CH_3) ppm.

3-Methyl-4-(4-methylbenzylidene)isoxazol-5(4H)-one (***4c***). FTIR (KBr, ν_{max}): 2924 (CH), 1731 (C=O), 1599, 1407 (C=C), 1110 (C–O), 776 (CH) cm^{-1}; ^1H NMR (300 MHz, $CDCl_3$): δ_H 8.32 (d, J = 7.95 Hz, 2H, H–Ar), 7.41 (s, 1H, C=CH), 7.35 (d, J = 7.68 Hz, 2H, H–Ar), 2.46 (s, 3H, Me), 2.31 (s, 3H, CH_3) ppm; ^{13}C NMR (75 MHz, $CDCl_3$): δ_C 168.2 (C=O), 161.2 (C=N), 150.0, 145.7, 134.1, 130.9, 129.9, 118.3, 22.1 (Me), 11.6 (CH_3) ppm.

4-(3-Methoxybenzylidene)-3-methylisoxazol-5(4H)-one (***4e***). FT-IR (KBr), ν (cm^{-1}): 3422 (=CH), 2946 (CH), 1738 (C=O), 1614 (C=N), 1438, 1569 (C=C), 1177, 1275 (C–O); ^1H NMR (300 MHz, DMSO-d_6): δ_H 8.20 (s, 1H, H–Ar), 7.96 (s, 1H, C=CH), 7.95 (d, J = 8.10 Hz, 1H, H–Ar), 7.54 (t, J = 8.00 Hz, 1H, H–Ar), 7.28–7.24 (m, 1H, H–Ar), 3.83 (s, 3H, OMe), 2.30 (s, 3H, CH_3) ppm; ^{13}C NMR (75 MHz, DMSO-d_6): δ_C 168.3 (C=O), 162.7 (C=N), 159.5, 152.1 (C–O), 134.1, 130.4, 127.1, 120.7, 119.4, 116.8, 117.9, 55.7 (OMe), 11.7 (CH_3) ppm.

3-Methyl-4-(4-methoxybenzylidene)isoxazol-5(4H)-one (***4f***). FTIR (KBr, ν_{max}): 3447, 2924 (CH), 1731 (C=O), 1624 (C=N), 1599, 1427, 1407, 1380 (C=C), 1187, 1110 (C–O), 993, 879, 776, 499 cm^{-1}; ^1H NMR (500 MHz, $CDCl_3$): δ_H 8.46 (d, J = 8.95 Hz, H–Ar), 7.85 (s, 1H, C=CH), 7.03 (d, J = 8.95 Hz, 2H, ArH), 3.93 (s, 3H, OMe), 2.29 (s, 3H, CH_3) ppm; ^{13}C NMR (75 MHz, $CDCl_3$): δ_C 169.0 (C=O), 164.7, 162.7 (C=N), 151.7 (C–O), 137.3, 126.2, 115.6, 115.1, 56.3 OMe, 11.7 (CH_3) ppm.

4-(3,4-Dimethoxybenzylidene)-3-methylisoxazol-5(4H)-one (***4h***). FT-IR (KBr), ν (cm^{-1}): 3409 (=CH), 2841 (CH), 1732 (C=O), 1562 (C=N), 1432, 1464 (C=C), 1177, 1275 (C–O); ^1H NMR (300 MHz, DMSO-d_6): δ_H 8.50 (s, 1H, H–Ar), 8.03 (dd, J_1 = 1.95 Hz, J_2 = 6.60 Hz, 1H, H–Ar), 7.85 (s, 1H, C=CH), 7.21 (d, J = 8.58 Hz, 1H, H–Ar), 3.09 (s, 3H, OMe), 3.08 (s, 3H, OMe), 2.26 (s, 3H, CH_3) ppm; ^{13}C NMR (75 MHz, DMSO-d_6): δ_C 169.2 (C=O), 162.7 (C=N), 154.8, 152.1, 148.7 (C–O), 131.5, 126.4, 115.8, 115.4, 116.8, 111.9, 56.4, 55.8 (OMe), 11.7 (CH_3) ppm.

4-(4-(Dimethylamino)benzylidene)-3-methylisoxazol-5(4H)-one (***4i***). FTIR (KBr, ν_{max}): 2924 (CH), 1713 (C=O), 1583 (C=N), 1527, 1437, 1410, 1383 (C=C), 1204, 1103 (C–O), 991, 873, 775, 507 cm^{-1}; ^1H NMR (500 MHz, DMSO): δ_H 8.46 (s, 2H, H–Ar), 7.51 (s, 1H, C=CH), 6.86 (s, 2H, ArH), 3.14 (s, 6H, NMe), 2.21 (s,

Table 1 Structural and textural parameters of SBA-15 and Cu/TCH@SBA-15

Sample	M^a (%)	$S_{BET}{}^b$ (m^2 g^{-1})	$V_{BJH}{}^c$ (cm^3 g^{-1})	$D_{BJH}{}^d$ (nm)	$V_{HKM}{}^e$ (cm^3 g^{-1})	$M_{pd}{}^f$ (nm)
SBA-15	—	629.63	0.836	5.11	0.258	5.079
Cu/TCH-pr@SBA-15	24	168.48	0.441	9.56	0.082	9.743

[a] Initial percentage of copper ions. [b] Specific surface area. [c] Pore volume. [d] Pore size (calculated from the adsorption branch). [e] Maximum pore volume at p/p° = 0.172869793 (estimated using the Horvath–Kawazoe method). [f] Mean pore diameter ($4V/A$ by BET).

Table 2 Optimizing the reaction conditions for the synthesis of 3-methyl-4-(4-methoxybenzylidene)isoxazol-5(4*H*)-one

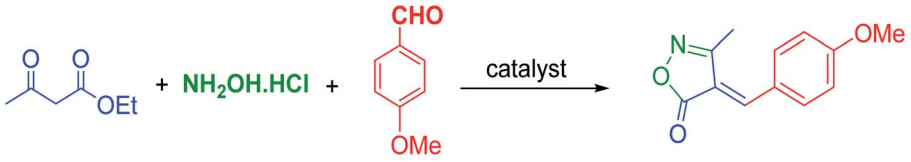

Entry	Catalyst loading (W%)	Solvent	Temperature (°C)	Time (min)	Yield[a] (%)
1	10	H_2O/EtOH (9 : 1)	Rt	30	70
2	10	EtOH	Rt	60	45
3	10	H_2O	Rt	60	45
4	5	H_2O/EtOH (9 : 1)	Rt	30	70
5	2.5	H_2O/EtOH (9 : 1)	Rt	35	70
6	2.5	H_2O/EtOH (9 : 1)	50	30	75
7	2.5	H_2O/EtOH (9 : 1)	80	15	87
8	2.5	H_2O/EtOH (9 : 1)	80	20	85
9	2.5	—[b]	50	12	75
10	**2.5**	—	**80**	**8**	**95**
11	2.5	—	100	8	95
12	1.5	—	80	10	65
13	5	—	80	8	90
14	SBA-15 (2.5)	—	80	30	10
15	TCH@SBA-15 (2.5)		80	30	20
16	—	—	80	60	10

[a] Isolated yield. [b] Solvent-free.

3H, CH_3) ppm; ^{13}C NMR (500 MHz, DMSO): δ_C 170.3 (C=O), 162.6 (C=N), 154.8, 150.9 (C–O), 138.0, 121.5, 112.1, 109.5, 39.6 ($N(CH_3)_2$), 11.8 (CH_3) ppm.

*4-(2-Hydroxybenzylidene)-3-methylisoxazol-5(4H)-one (**4k**).* IR (KBr), ν (cm^{-1}): 3187, 3416 (OH, =CH), 2854 (CH), 1738 (C=O), 1688 (C=N), 1458, 1575 (C=C), 1164, 1269 (C–O); ^{1}H NMR (300 MHz, DMSO-d_6): δ_H 11.05 (br, 1H, OH), 8.73 (d, J = 6.63 Hz, H–Ar), 8.08 (s, 1H, C=CH), 7.51 (m, 1H, H–Ar), 7.01–6.90 (m, 2H, H–Ar), 2.25 (s, 3H, CH_3) ppm; ^{13}C NMR (75 MHz, DMSO-d_6): δ_C 168.7 (C=O), 162.6 (C=N), 160.1, 145.5 (C–O), 137.2, 132.7, 119.9, 119.5, 116.8, 116.5, 11.6 (CH_3) ppm.

Table 3 Synthesis of 3-methyl-4-aryl isoxazole-5(4*H*)-ones (**4a–l**) under solvent-free conditions

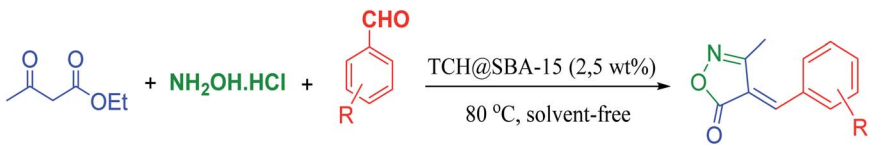

Entry	R	Time (min)	Product	Yield[a] (%)	Mp (°C)	Lit. mp (°C)
1	H	8	**4a**	90	137–138	140–142 (ref. 12)
2	3-Me	10	**4b**	90	145–147	141–142 (ref. 29)
3	4-Me	7	**4c**	92	131–132	132–133 (ref. 28)
4	2-OMe	8	**4d**	95	160–162	159–160 (ref. 13)
5	3-OMe	10	**4e**	89	134–136	130–132 (ref. 30)
6	4-OMe	8	**4f**	95	176–177	173–175 (ref. 12)
7	2,5-OMe	7	**4g**	96	174–176	178–179 (ref. 12)
8	3,4-OMe	8	**4h**	92	138	134–136 (ref. 8)
9	$N(Me)_2$	8	**4i**	95	218–220	222–223 (ref. 12)
10	4-Cl	12	**4j**	85	135–136	128–130 (ref. 31)
11	2-OH	8	**4k**	92	195–196	196–198 (ref. 12)
12	2-OH, 5-Br	12	**4l**	89	203–205	199–201 (ref. 36)

[a] Isolated yield.

3-Methyl-4-(5-bromo-2-hydroxybenzylidene)isoxazol-5(4H)-one (4l). FTIR (KBr, ν_{max}): 3421, 3150, (OH), 2900 (CH), 1751 (C=O), 1602, 1557, 1481, 1404, (C=C), 1292, 1280, 1105 (C–O), 991, 825, 773, 778 (CH) cm^{-1}; ^1H NMR (500 MHz, DMSO): δ_H 11.33 (br, 1H, OH), 8.92 (s, 1H, H–Ar), 7.95 (s, 1H, C=CH), 7.63 (d, J = 6.96 Hz, 1H, H–Ar), 6.99 (d, J = 7.53 Hz, 1H, H–Ar), 2.26 (s, 3H, CH_3) ppm; ^{13}C NMR (500 MHz, DMSO): δ_C 168.6 (C=O), 162.5 (C=N), 159.1 (C–OH), 143.6, 138.9, 134.3, 121.5, 118.8, 118.4, 110.5 (C–Br), 11.6 (CH_3) ppm.

3. Result and discussion

3.1. Preparation and characterization of Cu/TCH-Pr@SBA-15 nanocatalyst

The catalyst Cu/TCH-pr@SBA-15 was synthesized according to Scheme 2. SBA-15 was functionalized with organosilane precursor 3-chloropropyltriethoxysilane (CPTES) according to the reported method.[26] The resulting SBA-15-Cl was functionalized with a TCH ligand followed by complexation with $Cu(OAc)_2$ to afford the supported Cu catalyst on nanoporous SBA-15. Cu/TCH-pr@SBA-15 was characterized using different techniques, which are discussed below.

In order to show the functional groups of the nanocomposites, the FT-IR spectra of unmodified and modified SBA-15 were analyzed. The FT-IR spectrum of SBA-15 nanoparticles in Fig. 2(a) shows a broad band at 3431 cm^{-1}, which is due to the stretching vibrations of the Si–OH groups. The absorption bands at 1631 and 1097 cm^{-1} are characteristic of water bonded to the silica backbone and the asymmetric stretching of Si–O–Si, respectively.[26] The SBA-15-TCH spectrum in Fig. 2(b) has two bonds at 3273 and 3205 cm^{-1} that confirm the existence of NH_2 stretching vibrations. The bands stretching near 2959 and 1080 cm^{-1} can be attributed to the presence of C–H bonds from the $(CH_2)_3$ chains and C=S groups, respectively, in the TCH segment. The signals appearing at 1639 and 1497 cm^{-1} are attributed to the NH and CH bending vibrations, respectively. The FT-IR analysis in Fig. 2(c) shows a slightly different absorption behavior. The absorption band at 3429 cm^{-1} has become broader, and a shift in the NH bending frequency from 1639 cm^{-1} to 1620 cm^{-1} is observed. These results confirm that the Cu(II) ions were successfully immobilized on the surface of SBA-15-TCH.

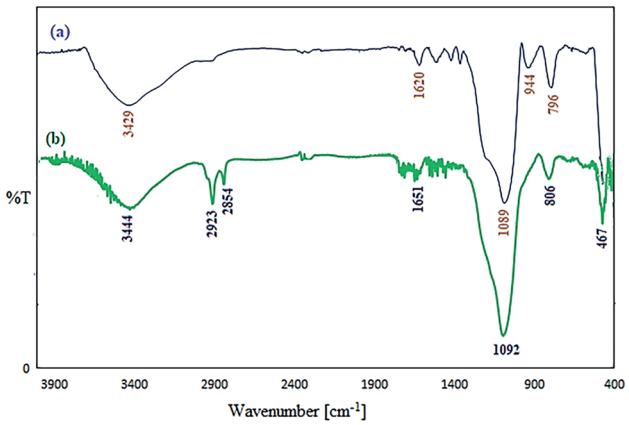

Fig. 5 FT-IR spectrum of the nano-catalyst (a) and recovered Cu/TCH-pr@SBA-15 (b) after the eighth cycle.

The FE-SEM image in Fig. 3(a) shows the surface morphology of SBA-15-TCH, with the nanoparticles having spherical nanostructures. The spherical structure of the nanoparticles is shown in Fig. 2(b and c), which is related to the FESEM images of Cu/TCH-pr@SBA-15. The TEM micrographs in Fig. 3(d) indicate the regular mesoporous channels of silica after modification.

The EDX analysis (in ESI†) confirms the presence of C, O, N, Si, S and Cu elements. Moreover, the amount of Cu loaded onto SBA-15 was estimated by atomic absorption spectroscopy to be 24% w/w (3.77 mmol g^{-1}).

Furthermore, the N_2 adsorption–desorption isotherm and BJH pore size distribution of the Cu/TCH-pr@SBA-15 nanocomposites are shown in Fig. 4.

The isotherm is classified as type IV, with a sharp capillary condensation step at a high relative pressure and H1 hysteresis loop, which reveals the presence of large channel-like pore structures with a narrow size range.[22] Also, based on the shape of its hysteresis, Cu/TCH-pr@SBA-15 has cylindrical pores and the initial nanostructure is retained after functionalization.[23] The hybrid inorganic–organic nanostructure shows a pore size distribution in the range of 10 nm. The structural data of the SBA-15 and Cu/TCH-pr@SBA-15 nanoparticles are summarized in Table 1. The BET surface area and pore volume of Cu/

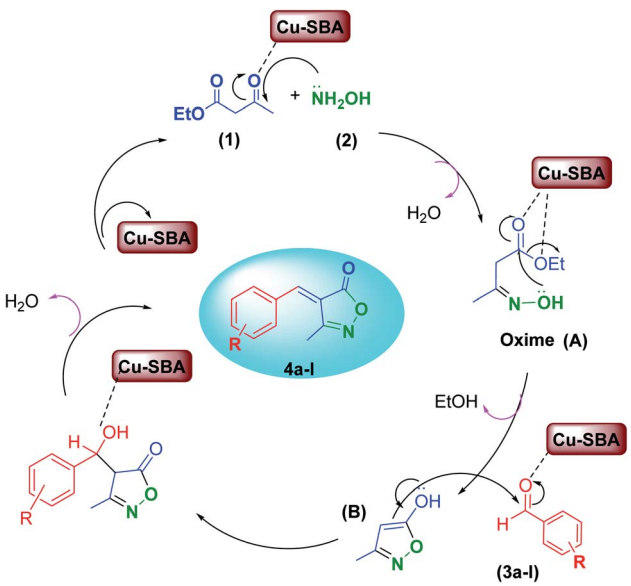

Scheme 3 Proposed catalytic cycle for the synthesis of 4-arylmethylene isoxazole-5(4*H*)-ones using Cu/TCH-pr@SBA-15.

Table 4 Study of catalyst recycling activity with the optimized reaction (time: 8 min, 80 °C) of isoxazolidinone synthesis (product **4f**)

Entry	1	2	3	4	5	6	7	8
Yield[a] (%)	95	93	90	88	87	87	85	80

[a] Isolated yield.

Table 5 Comparison of various catalysts for the synthesis of 4d

Entry	Catalyst	Conditions	Time (min)	Yield (%)
1	Nano MgO (3 mol%)	Water, rt	70	94 (ref. 33)
2	Sodium benzoate (10 mol%)	Water, rt	90	87 (ref. 17)
3	NH_2 MMT (0.01)	Distilled water, 30 °C	25	96 (ref. 13)
4	Nano Fe_2O_3 (1 mol%), AcONa	MW irradiation, solvent free	90	90 (ref. 32)
5	Sulfated polyborate (10 wt%)	Solvent free 80 °C	15	85 (ref. 34)
6	NBS (5 mol%)	Water, rt	80	95 (ref. 35)
7	DL-Tartaric acid (10 mol%)	Water, rt	60	85 (ref. 36)
8	Pyridine (100)	Water, ultrasound	60	82 (ref. 37)
9	NaS (5 mol%)	Ethanol, rt	90	88 (ref. 10)
10	Sodium azide (5 mol%)	Water, rt	210	90 (ref. 38)
11	**Cu/TCH@SBA-15 (2.5 wt%)**	**Solvent-free 80 °C**	**8**	**95 (this work)**

TCH@SBA-15 decreased due to the functionalization step of SBA-15. This reduction may be due to the significant loading of the complex into the mesoporous channels of SBA-15.[27]

3.2. Catalytic activities of Cu/TCH@SBA-15 in the solvent-free synthesis of 3,4-disubstituted isoxazole-5(4*H*)-one

In a preliminary experiment to find the optimal conditions for the synthesis of 4-arylidene-isoxazolidinones, we used 4-methoxy benzaldehyde, ethyl acetoacetate, and hydroxylamine hydrochloride as starting materials in the presence of Cu/TCH-pr@SBA-15 as a new nanocatalyst. To achieve the optimal conditions, the desired reaction was carried out in H_2O/EtOH (9 : 1) and solvent-free as a green process with different catalyst amounts and at various temperatures. As shown in Table 2, when 2.5 wt% of Cu/TCH-pr@SBA-15 was used, the desired product was formed in 95% yield at 80 °C under solvent-free conditions (Table 2, entry 10). The solvent-free technique is important for providing a green and eco-friendly system for catalytic processes. Also, in solvent-free reactions, as compared to reactions in solvent, the products formed are often pure enough to circumvent the need for difficult purification steps. Moreover, it was observed that the reaction conditions did not improve in the presence of SBA-15 and TCH@SBA-15 (Table 2, entries 14 and 15, respectively). On the other hand, without the nanocatalyst, the reaction did not proceed (Table 2, entry 16).

Under the optimized conditions, a study on a variety of aldehydes was carried out, and the representative results are presented in Table 3. Different aryl aldehydes were transformed into corresponding isoxazole-5(4*H*)-ones in excellent yields.

A proposed mechanism for the Cu-SBA-catalyzed synthesis of 4-arylidene-isoxazolidinones is shown in Scheme 3. In this catalytic cycle, Cu/TCH-pr@SBA-15 acts as a Lewis acid and activates the carbonyl groups in ethyl acetoacetate. Then, oxime (**A**) is generated *via* the condensation of ethyl acetate and hydroxylamine with the elimination of water molecule. Oxime was activated by the acidic nanocatalyst; then, cyclization of intermediate (**A**) occurs to generate (**B**) moiety. In the next step, Knoevenagel condensation occurred between (**B**) intermediate and aldehyde (**3a–l**) in the presence of the catalyst, which is followed by the elimination of H_2O to produce 3-methyl-4-aryl-methylene-isoxazole-5(4*H*)-one (**4a–l**).[13]

To demonstrate the reusability and recyclability of the nanocatalyst, after each cycle, the reaction mixture was allowed to cool and the catalyst was separated by filtration, washed with ethanol and ethyl acetate, and dried in an oven at 70 °C for 60 min prior to use. The model reaction proceeded with recovered Cu/TCH-pr@SBA-15 even after 8 cycles without any extension of the reaction time or marked loss in yield (Table 4).

The recovered nanocatalyst structure was confirmed with FT-IR spectroscopy. Fig. 5 shows that there is no difference in the FT-IR spectra of fresh and the five-times reused catalysts. Also, the Cu content of the nanocatalyst after the eighth reaction cycle was marginally decreased to 23.4% w/w (this reduction may be due to error in the experimental chemical analysis). As a result, the heterogeneous nature of the nanocatalyst is confirmed in this reaction, and very low copper leaching occurred.

A comparison of the Cu/TCH-pr@SBA-15 nano-mesoporous catalyst and some previous catalysts is listed in Table 5, revealing that this catalyst is superior to other reported catalysts in terms of yield, required amount of catalyst and reaction time.

4. Conclusion

In summary, we synthesized a heterogeneous organocatalyst, copper immobilized SBA-15 nanoparticles, for the three-component and solvent-free synthesis of isoxazole-5(4*H*)-ones (**4a–l**). This operationally simple and extremely general method can be efficiently applied to a wide variety of organic reactions with excellent yields. The nanocatalyst is recoverable up to eight cycles. Furthermore, the solvent-free and three-component synthesis makes this method relatively environmentally benign and a significant contribution to green chemistry.

Conflicts of interest

There are no conflicts to declare.

Acknowledgements

We gratefully acknowledge the financial support from the Payame Noor University for supporting this work.

References

1 D. Giomi, F. M. Cordero and F. Machetti, *Comprehensive Heterocyclic Chemistry III*, 2008, vol. 4, pp. 365–485.
2 J. Zhu, J. Mo, H. Z. Lin, Y. Chen and H. P. Sun, *Bioorg. Med. Chem.*, 2018, **26**, 3065–3075.
3 T. Karabasanagouda, A. V. Adhikari and M. Girisha, *Indian J. Chem.*, 2009, **48B**, 430–437.
4 M. M. M. Santos, N. Faria, J. Iley, S. J. Coles, M. B. Hursthouse, M. L. Martins and R. Moreira, *Bioorg. Med. Chem. Lett.*, 2010, **20**, 193–195.
5 A. Padmaja, C. Rajasekhar, A. Muranikrishna and V. Padmavathi, *Eur. J. Med. Chem.*, 2011, **46**, 5034–5038.
6 H. Kano, I. Adachi, R. Kido and K. Hirose, *J. Med. Chem.*, 1967, **10**, 411–418.
7 A. Srinivas, A. Nagaraj and C. S. Reddy, *Eur. J. Med. Chem.*, 2010, **45**, 2353–2358.
8 F. Saikh, J. Das and S. Ghosh, *Tetrahedron Lett.*, 2013, **54**, 4679–4682.
9 Y. Y. Kang, K. J. Shin, K. H. Yo, K. J. Seo, C. Y. Hong, C. S. Lee, S. Y. Park, D. J. Kim and S. W. Park, *Bioorg. Med. Chem. Lett.*, 2000, **10**, 95–99.
10 Q. Liu and X. Hou, *Phosphorus, Sulfur Silicon Relat. Elem.*, 2012, **187**, 448–453.
11 M. Mirzazadeh and G. H. Mahdavinia, *E-J. Chem.*, 2012, **9**, 425–429.
12 H. Kiyani and F. Ghorbani, *Heterolett*, 2013, **3**, 145–153.
13 J. Safari, M. Ahmadzadeh and Z. Zarnegar, *Catal. Commun.*, 2016, **86**, 91–95.
14 H. Kiyani and F. Ghorbani, *Open J. Inorg. Chem.*, 2013, **1**, 5–9.
15 K. Ablajan and H. Xiamuxi, *Chin. Chem. Lett.*, 2011, **22**, 151–154.
16 M. Ahmadzadeh, Z. Zarnegar and J. Safari, *Green Chem. Lett. Rev.*, 2018, **11**, 78–85.
17 Q. Liu and Y. N. Zhang, *Bull. Korean Chem. Soc.*, 2011, **32**, 3559–3560.
18 S. N. Madilla, S. Madilla, W. E. van Zyl and S. B. Jonnalagadda, *Res. Chem. Intermed.*, 2016, **42**, 2553–2566.
19 B. Karimi, S. Abedi, J. H. Clark and V. Budarin, *Angew. Chem.*, 2006, **118**, 4894–4897.
20 Z. Zarnegar and J. Safari, *New J. Chem.*, 2014, **38**, 4555–4565.
21 D. Sun, T. Misu, Y. Yamada and S. Sato, *Appl. Catal., A*, 2019, **582**, 117109.
22 J. Safaei Ghomi and A. Bakhtiari, *ChemistrySelect*, 2018, **3**, 12704–12711.
23 J. E. Sánchez-Velandia and A. L. Villa, *Appl. Catal., A*, 2019, **580**, 17–27.
24 B. Lu, Y. Ju, T. Abe and K. Kawamoto, *RSC Adv.*, 2015, **5**, 56444–56454.
25 (*a*) M. Kalhor, *Org. Chem. Res.*, 2015, **1**, 59–65; (*b*) M. Yarie, M. A. Zolfigol, S. Bagheri, D. A. Alonso, A. Khoshnood, M. Kalhor, Y. Bayat and A. Asgari, *New J. Chem.*, 2017, **41**, 4431–4440; (*c*) M. Kalhor, S. Banibairami and S. A. Mirshokraie, *Green Chem. Lett. Rev.*, 2018, **11**, 334–344.
26 (*a*) A. Alizadeha, M. M. Khodaei, D. Kordestania and M. Beygzadeh, *J. Mol. Catal. A: Chem.*, 2013, **372**, 167–174; (*b*) M. Kalhor, F. Rezaee-Baroonaghi, A. Dadras and Z. Zarnegar, *Appl. Organomet. Chem.*, 2019, **33**(5), e4784.
27 K. Sarkar, K. Dhara, M. Nandi, P. Roy, A. Bhaumik and P. Banerjee, *Adv. Funct. Mater.*, 2009, **19**, 223–234.
28 G. Ferouani, A. Nacer, N. Ameur, R. Bachir and C. Ziani-Cherif, *J. Chin. Chem. Soc.*, 2018, **65**, 459–464.
29 R. laroum and A. Debache, *Synth. Commun.*, 2018, **48**, 1876–1882.
30 U. Amol Khandebharad, R. Sarda Swapnil, H. Gill Charansingh and R. Agrawal Brijmohan, *Res. J. Chem. Sci.*, 2015, **5**, 27–32.
31 N. Irannegad-Gheshlaghchaei, A. Zare, S. S. Sajadikhah and A. Banaei, *Res. Chem. Intermed.*, 2018, **44**, 6253–6266.
32 S. Fozooni, N. Gholam Hosseinzadeh, H. Hamidianc and M. R. Akhgarb, *J. Braz. Chem. Soc.*, 2013, **24**, 1649–1655.
33 H. Kiyani and F. Ghorbani, *Res. Chem. Intermed.*, 2016, **42**, 6831–6844.
34 M. S. Patil, C. Mudaliar and G. U. Chaturbhu, *Tetrahedron Lett.*, 2017, **58**, 3256–3261.
35 H. Kiyani, A. Kanaani, D. Ajloo, F. Ghorbani and M. Vakili, *Res. Chem. Intermed.*, 2015, **41**, 7739–7773.
36 A. U. Khandebharad, S. R. Sarda, C. H. Gill and B. R. Agrawal, *Res. J. Chem. Sci.*, 2015, **5**, 27–32.
37 Q. F. Cheng, X. Y. Liu, Q. F. Wang, L. S. Liu, W. J. Liu, Q. Lin and X. J. Yang, *Chin. J. Org. Chem.*, 2009, **29**, 1267–1271.
38 H. Kiyani and F. Ghorbani, *Org. Chem.*, 2013, **58**, 14948–14950.